OXFORD

ORIGINAL ARTICLE

An Orientation Map for Disparity-Defined Edges in Area V4

Yang Fang[1,2], Ming Chen[1,2], Haoran Xu[1,2], Peichao Li[1,2], Chao Han[1,2], Jiaming Hu[1,2], Shude Zhu[1,2], Heng Ma[2] and Haidong D. Lu[2]

[1]Institute of Neuroscience, Shanghai Institutes for Biological Sciences, Chinese Academy of Sciences, and University of Chinese Academy of Sciences, Shanghai 200031, China and [2]State Key Laboratory of Cognitive Neuroscience and Learning, IDG/McGovern Institute for Brain Research, and the Collaborative Innovation Center for Brain Science, Beijing Normal University, Beijing 100875, China

Address correspondence to Haidong D. Lu, State Key Laboratory of Cognitive Neuroscience and Learning, Beijing Normal University, Beijing 100875, China. Email: haidong@bnu.edu.cn

Abstract

Binocular disparity information is an important source of 3D perception. Neurons sensitive to binocular disparity are found in almost all major visual areas in nonhuman primates. In area V4, disparity processes are suggested for the purposes of 3D-shape representation and fine disparity perception. However, whether neurons in V4 are sensitive to disparity-defined edges used in shape representation is not clear. Additionally, a functional organization for disparity edges has not been demonstrated so far. With intrinsic signal optical imaging, we studied functional organization for disparity edges in the monkey visual areas V1, V2, and V4. We found that there is an orientation map in V4 activated by edges purely defined by binocular disparity. This map is consistent with the orientation map obtained with regular luminance-defined edges, indicating a cue-invariant edge representation in this area. In contrast, such a map is much weaker in V2 and totally absent in V1. These findings reveal a hierarchical processing of 3D shape along the ventral pathway and the important role that V4 plays in shape-from-disparity detection.

Key words: binocular disparity edge, macaque monkey, optical imaging, orientation map, visual cortex

Introduction

Binocular disparity is the small differences in the visual field seen by the 2 eyes. Many animals, including humans, use this information to reconstruct the 3D visual world, along with other 3D cues (e.g., shading, occlusion, and size). In nonhuman primates, neurons sensitive to binocular disparities are found in most visual areas (Parker 2007). Disparity neurons in the dorsal visual area MT code absolute disparity in center-surround surfaces (Uka and DeAngelis 2006) but relative disparity in transparent surfaces (Krug and Parker 2011). These neurons are mainly involved in coarse disparity discriminations (DeAngelis et al. 1998; Uka and DeAngelis 2006; Chowdhury and DeAngelis 2008). In contrast, disparity neurons in the ventral areas (e.g.,

V4) are more sensitive to relative disparity (Umeda et al. 2007) and contribute to fine stereopsis (Uka et al. 2005; Shiozaki et al. 2012).

The processing of shape-from-disparity may start as early as V2, where some neurons are sensitive to disparity edges (DE), edges that are defined purely with binocular disparity (von der Heydt et al. 2000; Qiu and von der Heydt 2005; Bredfeldt and Cumming 2006; Bredfeldt et al. 2009). In the IT cortex, neurons are found that respond to disparity-defined 2D (Tanaka et al. 2001) or 3D shapes (Janssen et al. 1999, 2000a, 2000b, 2001; Uka et al. 2000; Verhoef et al. 2010, 2016). V4 is believed to be a key area linking the earlier visual cortex (V1 and V2) and high-level temporal cortex (e.g., IT). However, neurons sensitive to DE

have not been reported in this area, although their existence is expected. It is also unknown whether neurons respond to DE in V2 and higher areas form any functional organizations, for example, orientation maps. Topographic orientation maps have been observed in many visual areas, elicited either by luminance edges (LE) ([Ts'o et al. 1990](#); [Tanigawa et al. 2010](#)) or by second-order stimuli such as illusory contours ([Ramsden et al. 2001](#); [Pan et al. 2012](#)) and motion contours ([Chen et al. 2016](#)). Although an orientation map for DE has not been demonstrated yet, it is logical to expect that it may exist somewhere along the disparity-processing pathways.

In areas V2 and MT, neurons preferring similar disparity are clustered and form near-far disparity maps ([DeAngelis and Newsome 1999](#); [Chen et al. 2008](#); [Ts'o et al. 2009](#)). In contrast, disparity maps were not observed in V1 ([Chen et al. 2008](#); [Kara and Boyd 2009](#)). In other extrastriate areas such as V3, V3A, V4, and IT, disparity-sensitive neurons also tend to cluster, as suggested by single-cell recordings ([Adams and Zeki 2001](#); [Watanabe et al. 2002](#); [Yoshiyama et al. 2004](#); [Tanabe et al. 2005](#); [Anzai et al. 2011](#)). However, direct evidence for near-far disparity maps in these areas has not been reported so far.

Here, we studied cortical functional architectures for binocular disparity with intrinsic signal optical imaging. We imaged cortical regions (V1, V2, and V4) in the same imaging chamber in both anesthetized and awake monkeys. We found not only responses to DE in area V4 but also orientation maps for such responses. In contrast, such orientation maps were only weakly present in V2 and were absent in V1.

Materials and Methods

All procedures were performed in accordance with the National Institutes of Health Guidelines and were approved by the Institutional Animal Care and Use Committees (Institute of Neuroscience, Chinese Academy of Sciences, and Beijing Normal University).

Cases and Experimental Sessions

A total of 7 hemispheres (cases) from 5 adult male macaque monkeys (*Macaca mulatta*, 5–10 years old) were examined. Two hemispheres from 1 monkey were not analyzed because this monkey had an eye-rotation after anesthesia and paralysis; thus, an eye alignment could not be established. The other 5 cases from 4 monkeys were all used in this study. The case information is summarized in Supplementary Table S1. Among these 5 cases, 4 cases from 3 monkeys were imaged in an anesthetized condition and 1 case from 1 monkey was imaged in an awake condition. Three cases (2 anesthetized and 1 awake) were imaged for multiple experimental sessions. The other 2 cases were mainly used for other projects and were only imaged for 1 session. For cases imaged for multiple sessions, sessions with the best signal-noise ratios were chosen as representative sessions for these cases.

Animal Preparation and Optical Imaging

Chronic imaging chambers were implanted under sterile conditions and isoflurane (1–2.5%) anesthesia ([Chen et al. 2002](#); [Li et al. 2013](#)). Lidocaine was applied at pressure points and surgical incisions for local analgesia during the implanting procedures. The size of the chamber was 24 mm in diameter, which allows an 18-mm imaging field-of-view. The chambers were positioned laterally so that the medial edge of the chamber was

approximately 22 mm from the midline (Fig. [1A](#)). The lunate sulcus was normally in the middle of the chamber window to allow a view of 3 visual areas (V1, V2, and V4; see Fig. [1B](#)). The eccentricity of the visual space corresponding to the exposed visual cortex was approximately 0°–2° for V1 and V2 and approximately 0°–10° for V4.

After a chronic chamber was implanted, the animal was imaged repeatedly at an interval of 1–2 weeks between 2 consecutive experimental sessions. During optical imaging, the monkeys were anesthetized with Propofol (induction: 5 mg/kg, maintenance: 5 mg/kg/h, i.v.), paralyzed with vecuronium bromide (induction: 0.25 mg/kg, maintenance: 0.05 mg/kg/h, i.v.) and artificially respired. Lidocaine was applied at pressure points for local analgesia. The pupils were dilated (atropine sulfate 1%), and the eyes were fitted with contact lenses of an appropriate curvature to focus on a stimulus screen 57 cm from the eyes. Images of cortical reflectance changes (intrinsic hemodynamic signals) were acquired (Imager 3001, Optical Imaging Inc.) with 632-nm illumination at a frame rate of 4 Hz. One single imaging trial lasted 4 s, during which 16 image frames were collected. The image size was either 540×654 pixels (for anesthetized monkey imaging) or 504×504 (for the awake monkey), representing either a 15.3×18.5 or a 15×15 mm^2 field-of-view. Some of the images shown in the figures were cropped for a better view.
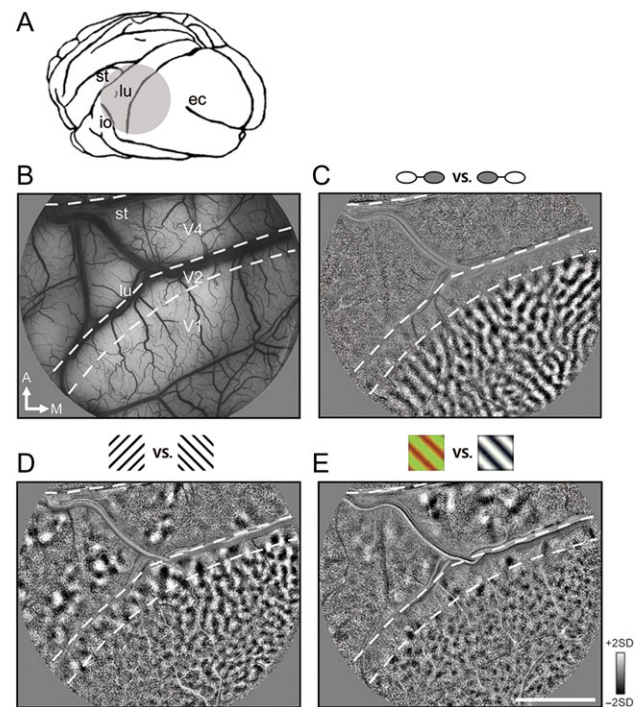

Figure 1. Basic functional maps in monkey visual areas V1, V2, and V4. (A) Illustration of a monkey brain and imaging window location (gray disk) on the left hemisphere. Sulcus abbreviations: lu, lunate; st, superior temporal; ec, external calcarine; io, inferior occipital. (B) A surface blood vessel map of the imaging window in an example case. Dashed lines separate different visual areas. A, anterior; M, medial. (C–E) Basic functional maps (SVM maps) of the same cortical regions shown in B obtained by comparing cortical responses to 2 types of visual stimulation (illustrated on the top of each map). (C) An ocular dominance map obtained by comparing cortical activation during left-eye stimulation and right-eye stimulation. Only area V1 shows ocular dominance columns. (D) A 45° vs. 135° orientation map shows the orientation-preferring domains in all 3 visual areas. (E) A color versus luminance map shows color-preferring domains: blobs in V1, thin stripes in V2 and globs in V4. Scale bar in E: 5 mm, applies to B–E.

Awake Monkey Optical Imaging

Awake imaging procedures have been described in detail in a previous publication (Chen et al. 2016). Briefly, a monkey was trained to perform a simple fixation task. The fixation dot was a 0.3° red spot, and the fixation window was 1.5° in diameter. One eye was monitored with an infrared camera (Eyelink 1000, SR Research), and we confirmed that the eye position was stable on the X-axis before and during the stimulus presentation. Some small eye position shifts on the Y-axis were observed. After a careful check and consulting with the eye-tracker manufacturer, we determined that those shifts were due to pupil size changes (in responding to the screen luminance change) and were not real eye movement. In each trial, the monkey was required to fixate for 4.5 s to obtain a juice reward. Cortical responses were imaged 0.5 s after the initiation of fixation and continued for 4 s. Visual stimuli were presented 0.5 s after the initiation of imaging and lasted for 3.5 s. The interval time between each trial was 6 s.

Dichoptic View and Binocular Alignment

In anesthetized monkey imaging, dichoptic stimulation was achieved by using a pair of 7° prisms in front of the monkey's eyes; each prism bent light for 7° horizontally (Xu et al. 2016, also see Fig. 2A). The 2 eyes' views diverged horizontally, so 2 patches of visual stimuli for the 2 eyes could be presented on the left and right halves of the CRT screen (width: 40°, height: 30°). The visual field locations of the exposed V1 were determined with an imaging procedure (Lu et al. 2009). Briefly, single horizontal and vertical bars at different screen locations were present to each eye alone (through the prism), and the V1 retinotopic activation was measured (Figs. S1 and S2). Precise eye alignment can be achieved by flip-flopping left- and right-eye activation images, during which a 0.1° offset can be easily noticed (Lu et al. 2009). Relative rotations between the left and right eyes were measured similarly by comparing 2 monocular bar-activation patterns in V1 or by comparing 2 monocular orientation maps. After the stimulus center locations for the
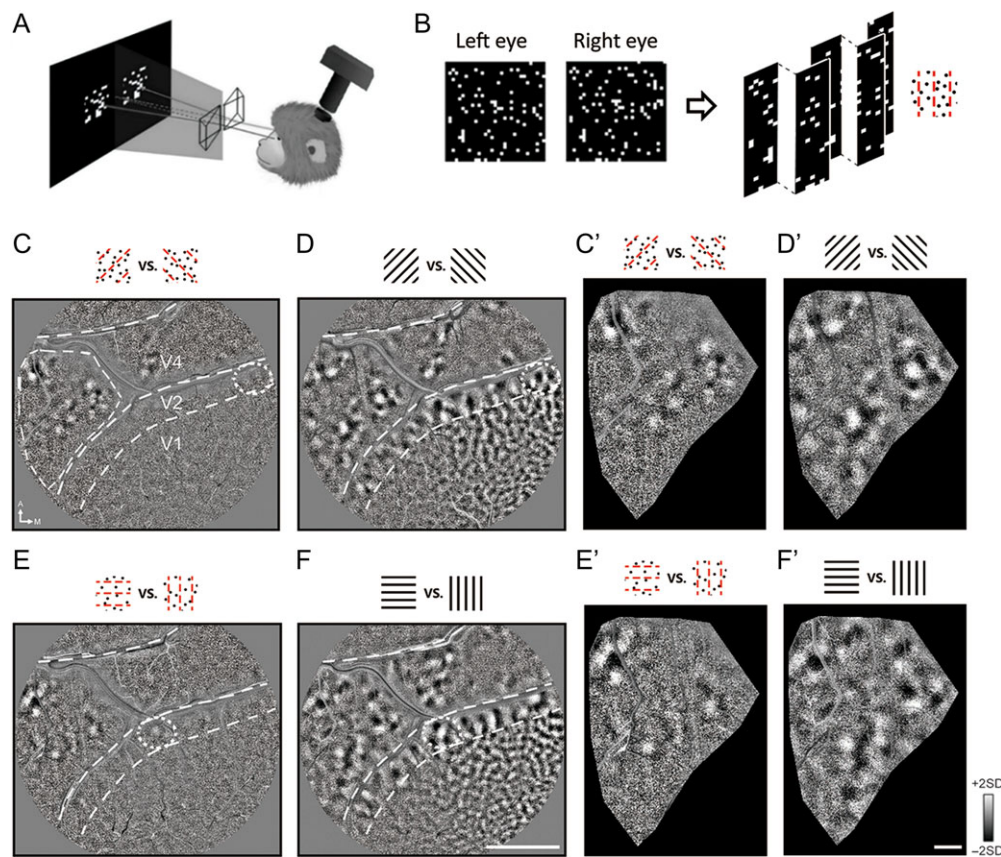

Figure 2. Orientation maps obtained with disparity-defined edges (DE). (A) An illustration of the imaging setup and dichoptic stimulus presentation method in the anesthetized monkey experiments. Two patches of random dots on the stimulus screen were converged by a pair of prisms to form a stereo view. A black curtain in the middle was used to separate 2 eyes' visual fields. (B) An illustration of the DE stimuli used in this study. The monocular RD patches did not contain any monocular edge cues. After convergence, each stimulus contained 2 sets of RD strips located at 2 different depth planes (0° and –0.2° depth in the example shown). The orientation of the strips was one of following (0°, 45°, 90°, and 135°). A vertical orientation (90°) DE is shown in this illustration. (C) A DE orientation map obtained by comparing cortical responses during 45° DE stimulation and 135° DE stimulation. There are separate 45°-preferring domains (black patches) and 135°-preferring domains (white patches) in area V4, but this is not apparent in areas V1 or V2 (except for several weakly presented ones in V2, indicated by a dotted circle). The outlined region in V4 is magnified in (C′). (D) An orientation map for luminance-defined edges (LE) obtained by comparing responses to 45° and 135° luminance gratings. This map is the same as the one shown in Figure 1D. All 3 areas (V1, V2, and V4) exhibit orientation-specific responses to the LE stimuli. A dotted circle in V2 indicates the same outlined region in C for comparison. (E and F) Similar to C and D, orientation maps obtained with another set of orthogonal gratings (0° and 90°) from the same cortical areas. Similarly, V4 exhibits a DE orientation map that is consistent with the V4 LE orientation map. No clear DE orientation map is observed in V1 and V2, except several V2 regions may exhibit some weak responses (dotted circle). (C′–F′) Magnified views of a region in V4 (outlined in C) for panels C–F for detailed comparison. Stimulus icons are the same as C–F. Although the maps obtained with LE are stronger than those with DE, the V4 maps obtained with DE and LE stimuli exhibit similar spatial patterns. Note that each map was clipped to ±2 SD of that map; thus, the contrast of each map does not reflect its real signal strength. Scale bar in F: 5 mm, applies to C–F. Scale bar in F′: 1 mm, applies to C′–F′.

exposed V1 region were determined, the stimulus center locations for the exposed V4 region were estimated by adding 1°–3° (horizontally) and 1°–3° (vertically) to the measured V1 center locations in directions away from the fovea for both patches. The eye positions were checked with this method every hour during the binocular imaging, and stimulus locations were adjusted when an eye drift was detected.

In awake imaging, dichoptic stimulation was achieved by using a pair of LCD shutter glasses (modified from FE-1 Shutter Goggles, Cambridge Research Systems Ltd.). The left-eye images and right-eye images were presented at the same screen location for even and odd frames, respectively. The shutter glasses were synchronized with the CRT stimulus monitor, which operated at a frame rate of 100 Hz. Each shutter only opened when even or odd frames were presented (50 Hz). When the CRT monitor was operated at even or odd frames, the screen luminance for white stimuli was 41.5 cd/m^2 (measured without shutter glasses). At that time, the luminance level measured through an open shutter was 11.1 cd/m^2 (transparent efficiency: 26.7%); the luminance level measured through a closed shutter was 0.83 cd/m^2 (crosstalk: 2%). This crosstalk value was small and did not produce detectable cortical activations in control tests.

Visual Stimulus

Visual stimuli were created using ViSaGe (Cambridge Research Systems Ltd.) and displayed on a calibrated 21-inch CRT monitor (SONY CPD-G520) placed 57 cm in front of the eyes. Unless otherwise specified, the luminance for the white pixels was 80 cd/m^2 and was 0.3 cd/m^2 for the black background.

Ocular Dominance, LE Orientation, and Color Stimuli

To obtain ocular dominance and orientation preference maps, we used full-screen drifting black–white rectangle-wave gratings. The duty cycle of the gratings was 0.2 (20% white), and the spatial frequency (SF) was 1.5 cycles/deg for ocular dominance map imaging and 1.2 cycles/deg for orientation map imaging. Gratings were drifting at 5.33°/s (8 Hz) and were presented in a randomly interleaved fashion in 1 of 8 directions (0°, 45°, 90°, 135°, 180°, 225°, 270°, or 315°). The initial phase of the gratings was randomly selected.

Color stimuli contained 4 conditions, including 2 isoluminant red–green sinewave gratings (orientation 45° and 135°) and 2 black–white gratings of the same SF (0.2 cycles/deg) and speed (5.33°/s). The drifting direction was randomized.

DE Stimulus

DE stimuli were made from 2 square patches of random dots (RD). Each was 10° × 10° in size and contained white dots on a black background (Fig. 2B, also see Movie S1). Dots were 1 pixel (~0.05°) in size and covered 15% of the patch surface. Taking 1 frame of the stimulus as an example, the left- and right-eye patches were based on the same RD template. The right-eye patch was then divided into several strips (e.g., vertical strips), and the RDs in half of the strips (even or odd strips) were shifted horizontally to create binocular disparity with the corresponding strips in the left-eye patch. The horizontal shifts were either towards the left or right and induced either a near (−) or far (+) depth for these strips after binocular merging. The other nonshifted strips always had a zero disparity. The gaps due to horizontal shifts were filled with new RD, and the additional dots in the new overlapping areas were removed. Adjustable parameters included the disparity level of half of the strips

(−0.3°, −0.2°, −0.1°, 0.1°, 0.2°, 0.3°); SF of the DE (0.8, 1.2, or 1.6 cycles/deg, corresponding to strip widths of approximately 0.6°, 0.4°, 0.3°); and the orientation of the DE (0°, 45°, 90°, 135°). To achieve stronger activation of the visual cortex, all RD of the 2 patches were drifting coherently within the patches at a speed of 4°/s (Movie S1).

A typical DE imaging run contained 11 or 19 conditions in which the strip disparity level (−0.2°) and strip SF (1.2 cycles/deg) were the same for all conditions. Either 2 orthogonal DE orientations (usually 45° and 135°) or 4 equally spaced DE orientations (0°, 45°, 90°, and 135°) were tested. Each DE orientation was tested with 4 RD drifting directions to reduce the adaptation effect. The drifting directions were always at a 45° angle with respect to the DE orientations to avoid interactions (if any) with the DE orientation. So when 2 orthogonal DE conditions were compared, their RD motion components were identical and could be subtracted out. In addition, each run contained 3 "blank" conditions: a zero-disparity RD (both eyes the same) drifting toward either the left or right and a black screen condition. In additional runs, we also modulated different parameters to test the consistency of V4 DE coding (Fig. S7).

Matching Edge Stimulus

By introducing strips of different degrees of binocular matching to a DE stimulus, we tested how such matching information contributes to the cortical orientation responses (Fig. 5E). Matching edge stimuli were constructed in a similar way as the DE stimuli, except that the one set of RD strips contained binocularly unmatched RD (binocularly uncorrelated RD). These unmatched RD strips were interleaved with binocularly matched-RD strips (zero disparity). Thus, this stimulus contained virtual edges separating binocular matching and nonmatching strips. Perceptually, such edges are perceivable but much weaker than the DEs.

DE With Vertical Disparity

As a control stimulus, we also tested DE stimuli constructed with vertical disparity (Fig. 5H). The stimulus parameters were the same as in DE stimuli except that RDs were shifted vertically between the 2 eyes.

DE With Anti-correlated RDs

In anti-correlated DE stimuli, the RD patches had a gray background (luminance value: 40 cd/m^2) containing half white dots (80 cd/m^2) and half black dots (0.3 cd/m^2), with a total dot density of 15%. Compared with regular correlated conditions, the signs of the dots (black vs. white) were reversed in anti-correlated stimuli between the left-eye and right-eye images (Fig. 6A,B). Other parameters were the same as in the regular (correlated) DE stimuli described above. For a direct comparison, a set of correlated DE stimuli were also constructed with black and white dots and tested in the same imaging run together with these anti-correlated DE stimuli.

Disparity Stimulus

Disparity stimuli were created to test the cortical responses to pure disparity information (near vs. far). A disparity stimulus was created in a similar way to the DE stimulus described above, except that there were no strips inside the patches. There was also a 10° × 10° square patch that contained RD of the same size and density as the standard DE stimulus. The differences were that the disparity stimulus contained one 8° × 8° center, which was presented at 1 of 5 possible depths: −0.2°, −0.1°, 0, +0.1°, or +0.2°. The surrounding dots beyond the center

square of 8° were always at zero disparity. There were also 2 types of blank conditions: binocularly uncorrelated RD conditions (in both the center and surrounding areas) and a "true blank" condition (black screen). RD were drifting coherently within the 10° × 10° patches at a speed of 4°/s in either the left or right directions (total of 13 conditions) or were refreshed by new RD patterns at 10 Hz (total of 7 conditions).

Awake Imaging Visual Stimulus

In awake monkey imaging, we used a pair of LCD shutter glasses to create a dichoptic view (described above). The RD patches in the left- and right-eye stimuli were the same as those used in the anesthetized imaging. The difference was that in awake imaging, the left- and right-eye stimuli were alternatively presented at the same screen location. For example, the left-eye stimuli were presented only in an odd number of the video frames, during which the left-eye shutter was open and the right-eye shutter was closed. Similarly, the right-eye stimuli were presented only in an even number of video frames while the right-eye shutter was open and the left-eye shutter was closed. The CRT screen was working at a frame rate of 100 Hz, and each eye's image was refreshed at 50 Hz. A typical DE imaging run contained 9 conditions, including 8 DE conditions (2 DE orientations combined with 4 drifting directions) and a blank condition (black screen with a fixation point). The 10° × 10° stimulus patch was presented at a center location of ($x = 4°$, $y = -4°$) (Fig. 4A) for the left hemisphere imaging. The stimulus was presented for 3.5 s, and the imaging started 0.5 s before the stimulus and lasted for 4 s.

Data Analysis

Support Vector Machine Maps

We used support vector machine (SVM) maps to show the differences in cortical activation between the 2 stimulus conditions. SVM is a pattern classification algorithm that has recently been used to extract a stimulus preference in fMRI images (Kamitani and Tong 2005) or optical imaging maps (Xiao et al. 2008; Chen et al. 2016). The Matlab SVM program was provided by Chih-Jen Lin (LIBLINEAR: A Library for Large Linear Classification, 2008; available at https://www.csie.ntu.edu.tw/~cjlin/liblinear/). For each stimulus condition, a percentage change map (dR/R) was first calculated using the following formula: $dR_i/R = (R_i - R_0)/R_0$, where R_i are the responses in single frames between frames 8 and 16 and R_0 are the average responses in frames 1–4. The resulting images were then used for SVM classification. One SVM weight map was obtained for 2 sets of images corresponding to the comparison conditions. In an SVM weight map, each pixel's gray value represents the relative contribution that this pixel makes to the classification (black or white indicates the identity of the stimulus to which it contributes, while gray indicates weak contribution). Unless otherwise specified, all SVM maps were high-pass filtered (mean circular filter, kernel size = 50 pixels or 2 mm) to remove low SF variations and were clipped at 2 SD on each side of the map median for display. All maps shown in the figures are SVM maps, except for Figure S1 (only dR/R subtraction maps were available due to few repeats) and Figure S3E,F, where comparisons between the SVM and t-test maps were made.

T-Test Maps

In addition to SVM maps, t-test maps were also calculated (Li et al. 2013). Similar to SVM maps, 2 sets of dR/R frames were calculated. A t-value was calculated for each pixel based on the following formula (paired t-test):

$$t_i = \frac{(C1_i - C2_i) \times \sqrt{N}}{S_i}$$

In this formula, $C1_i$ and $C2_i$ are the means of pixel i's dR/R values for conditions 1 and 2, S_i is the SD of ($C1_i - C2_i$), and $\sqrt{N}$ is the square root of the sample size (number of repeats). Maps based on t-values were called t-test maps. Compared with SVM maps, t-test maps exhibit more noise, especially in the blood vessel regions (Fig. S3). However, since pixel values in t-test maps are more meaningful (the t-value is equivalent to a signal-noise ratio), t-test maps were used in an analysis where a quantification was necessary (e.g., response profile calculation in Fig. 3I–L). Blood vessel regions were excluded from quantifications.

Response Profile

Population response profiles were calculated to assess the overall orientation response in a particular map, that is, which orientation domains were mostly activated (Basole et al. 2003; Chen et al. 2016). Briefly, the orientation angle map obtained from a vector analysis (Bosking et al. 1997) was used as the reference angle map. For a specific t-test map under examination, the top 40% of pixels in a magnitude map from a vector analysis were categorized into 20 orientation-selective groups (0°–180°) according to their orientation angles in the reference angle map. Pixel values within each group were then summed. The resulting response profile reflects whether a specific orientation-preferring group of pixels was activated in the map. We chose t-test maps for the response profile analysis instead of an SVM map because its pixel values are better related to the raw response. The maps were low-pass filtered (mean circular filter, kernel size = 5 pixels or 0.2 mm) and high pass filtered (mean circular filter, kernel size = 100 pixels or 4 mm). The resulting response profile (e.g., Fig. 3J) reflects whether a map contains specific orientation information. If a map has no spatial correlation to the corresponding orientation map (the reference angle map), which means this map has no specific orientation information, the profile will be flat. To evaluate the statistical significance of a particular response profile, we created shuffled datasets based on the real datasets and calculated their response profiles for comparison. To do that, we randomly selected half of the trials and switched the 2 sets of images to be compared in these trials. Then, these "switched" trials were put back with the other half of the "normal" trials and analyzed in a regular way. Since the "new" data contained images from mixed conditions, t-test maps obtained from these datasets mainly reflect random noise, and the response profiles are mainly flat. For each map, we repeated the shuffling 10 times and obtained 10 "shuffled" response profiles. Then, the original response profiles were compared with these corresponding shuffled profiles. If the amplitude of one meaningful response profile was significantly higher than the shuffled groups (larger than the 95% confidence level of the shuffled controls), we determined that this response was significant (labeled "*" on the curves). We also used the ratio between the response profile curve amplitude and corresponding average amplitude from shuffled curves as the "amplitude ratio" to evaluate the quality of the maps. For each imaging session, the amplitude ratio of the LE orientation map was defined as the "signal-noise ratio" to evaluate the imaging session qualities (e.g., Supplemental Table S1).
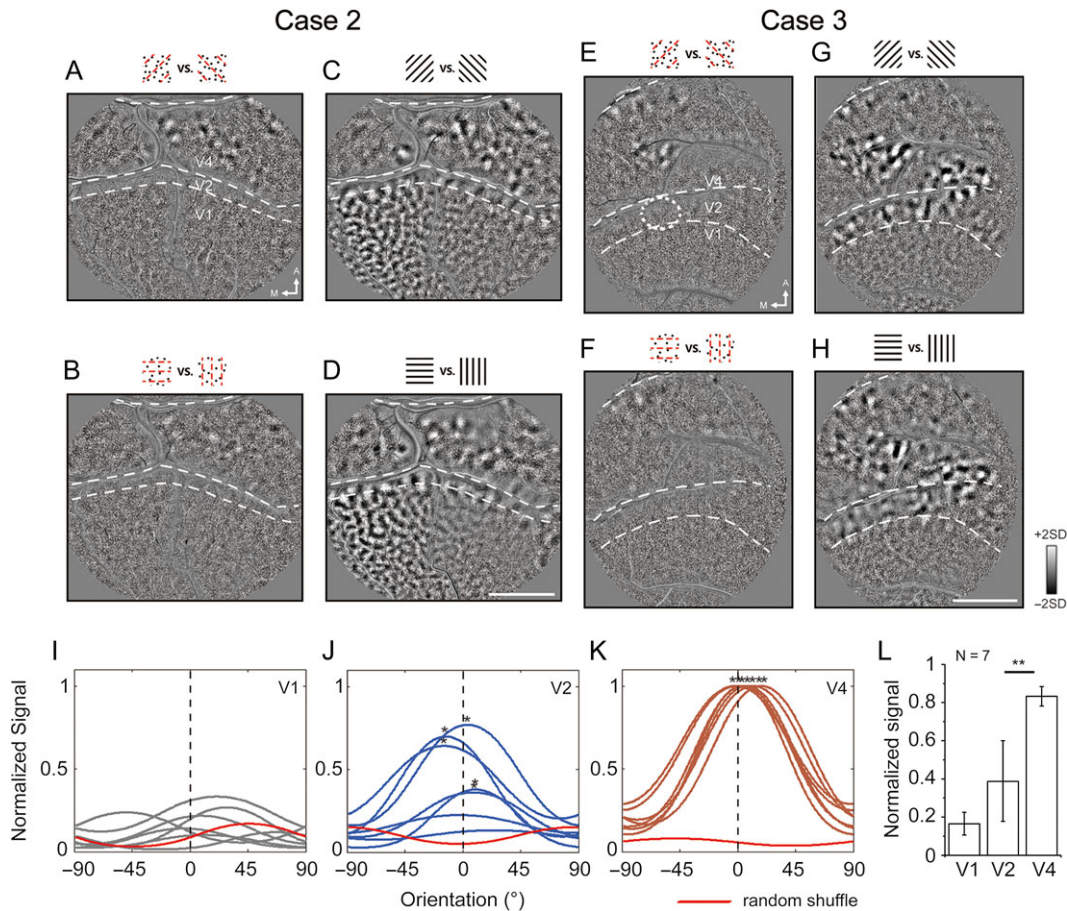
Figure 3. DE orientation maps from 2 other cases and quantitative analysis of the maps. (A–D) Maps from Case 2. Stimulus and plotting conventions are the same as Case 1, shown in Figure 2 C–F. (A and B) Two orientation maps obtained with DE stimuli. Only V4 exhibits orientation patterns. (C and D) Two orientation maps obtained with LE stimuli. All 3 areas have orientation patterns. Comparison of DE orientation maps and corresponding LE orientation maps show similar responses in V4 but not in V1 and V2. (E–H) Same as A–D, maps from Case 3. Similar trends as in Cases 1 and 2 were observed. A weak V2 DE response region is indicated (dotted circle in I). (I–K) Response profiles for DE orientation maps in all 4 cases. All curves were horizontally shifted so that 0 on the X axis represents the stimulus orientation. Curve amplitudes are t-values from corresponding t-maps and were normalized to the peak amplitude for V4 response. Note that Cases 1–3 each contribute 2 curves and that Case 4 contributes one curve since only one pair of orientations was tested, so there are 7 curves in total. An additional curve (red) in each panel is a representative shuffled control in each group. Curves with significant response amplitudes are labeled with "*" (amplitude larger than the 95% confidence level of the shuffled controls). (I) DE responses in V1 are close to the baseline and do not differ from the shuffled controls. (J) Some DE responses in V2 exhibit weak orientation tuning, and 5 out of 7 curves have response strengths (peak-trough) that are significantly larger than the shuffled controls. (K) DE responses in V4 exhibit strong orientation selectivity for the DE orientation in terms of both response strength and orientation selectivity (maximum responses at the stimulus orientation). (L) Average response strengths from response profiles in I–K. The response strength from V4 curves is significantly larger than those from V2. The V2 response strength is larger than V1, and this difference is close to significant. Error bar: SD. Scale bar in D: 5 mm, applies to A–D. Scale bar in H: 5 mm, applies to E–H.

Awake imaging data analysis was similar to that used for data collected with anesthetized subjects. Trials in which the animal broke fixation were excluded. All frames were aligned before analysis for correction of animal motion noise (Chen et al. 2016).

Results

Basic Functional Maps

In anesthetized conditions, area V4 was well activated by different types of visual stimuli. Figure 1 shows the imaged cortical regions and basic functional maps in Case 1. Basic functional maps for 2 other cases are shown in Figure S4. All functional maps are SVM weight maps obtained with an SVM pattern classifier that was trained to compare images from 2 stimulus conditions (Chen et al. 2016). The imaging chambers were positioned to include 3 visual areas (V1, V2, and V4) in the same field-of-view. Area V4 exposed on the surface was

identified based on sulcal features (Essen and Zeki 1978) to be between the lunate sulcus and the superior temporal sulcus. The border between areas V1 and V2 was determined by an ocular dominance map where only V1 exhibited ocular dominance columns (Fig. 1C). In all cases, we obtained clear orientation maps and color maps in area V4 (Fig. 1D,E and Fig. S4). The mean domain sizes (orientation: 532.5 μm; color: 663.7 μm) were similar to those previously reported (orientation: 542–570 μm; color: 527–600 μm) (Ghose and Ts'o 1997; Tanigawa et al. 2010; Li et al. 2013). Additionally, consistent with these previous reports, the orientation and color domains in V4 appeared to avoid each other and occupied different portions of V4.

DE Maps in V4

DE stimuli were made from two 10° × 10° patches of RD, presented on each side of a CRT screen and converged using a pair of prisms to form a fused binocular view (Fig. 2). To determine

the precise stimulus locations, we measured visual field locations for each of the 2 eyes with a bar imaging method (Lu et al. 2009; Xu et al. 2016). After being fused by the prisms, the DE stimuli contained near and far strips (illustrated in Fig. 2) oriented in 1 of 4 possible orientations (0°, 45°, 90°, or 135°). Figure 2 shows SVM weight maps from 1 example case (Case 1). Figure 2C is a DE orientation map based on a comparison of the responses to the 45° and 135° orientation conditions (45° vs. 135°). In this map, black and white pixels represent regions that were preferentially activated by 45° and 135° orientations. Clear patterns were observed in V4, and in some isolated regions in V2 (dotted circles in Fig. 2C,D), but were totally absent in V1 (see quantitative analysis in Fig. 3I–L). The V4 patterns are similar to the V4 orientation-preference domains obtained with luminance-defined edges (LE) (Fig. 2D). Figure 2C′,D′ shows magnified views of the same V4 regions (outlined in Fig. 2C) in Figure 2C,D. There are some local differences between these 2 maps, but the centers of the orientation domains are mostly in the same locations, and the spatial layouts are generally similar (Figs S5 and S6). The analysis also shows that the small local differences between the DE and LE orientation maps are mostly due to the weak signals in the DE orientation map (Fig. S5K–M). Note that each map was individually clipped (to ±2 SD of the map); thus, the differences in the signal strengths are not apparent in these maps. Detailed comparisons of signal strengths can be found in Figure S5K. In strong contrast to V4, V1 and V2 did not show clear orientation patterns for the DE stimuli, except for some weakly presented local patches in V2 (dotted circle in Fig. 2C). As a comparison, clear orientation maps for LE stimuli were obtained in these 2 areas in the same imaging session (Fig. 2D). We also obtained DE and LE orientation maps for 0° versus 90° orientations (Fig. 2E,F,E′,F′). Consistently, a clear DE orientation map was only observed in area V4 and generally had a spatial pattern similar to the corresponding LE orientation map.

In 5 cases we examined, V4 DE orientation maps were obtained in all cases and for multiple experimental sessions (see Supplementary Table S1). In Figure 3A–H, the DE orientation maps from Cases 2 and 3 are shown along with LE orientation maps. All of these cases showed a similar trend to Case 1: orientation maps for DE existed in area V4 and were consistent with the corresponding LE orientation maps. In contrast, DE maps were much weaker in V2 and were absent in V1.

To quantitatively measure the orientation selectivity of these maps, we used the response profile method (Basole et al. 2003). A response profile is a measurement used to quantitatively identify which orientation domains are preferentially activated in a difference map or a region in the map. A flat profile means that all orientation domains are equally activated (showing no orientation preference). Figure 3I–K show the orientation profiles for V1, V2, and V4 of all 4 anesthetized cases, as well as their shuffled controls (red curves; see Materials and Methods; only 1 representative curve is shown for each panel). All curves are sinewave-fitting curves ($R^2 > 0.5$). The stimulus orientations were aligned at 0° on the X axis. Curves were normalized to the V4 response peaks in the same case. It can be seen that the responses in V4 were the strongest among all 3 areas and that all V4 curves peaked at (or close to) the stimulus orientations. In contrast to the visual impression of the maps, many V2 curves also exhibited selective responses to the stimulus orientation. Thus, the response profile method appeared more sensitive than the visual inspection of the maps, likely due to the fact that it pools useful information from all the V2 pixels. For the V2 response profiles, 5 out of 7 curves had amplitudes (peak minus trough) that were significantly larger than

the shuffled controls (larger than the 95% confidence level of the shuffled control amplitudes, labeled with "*"). This is also consistent with the spatial correlation results in which V2 also showed a significant response (Fig. S6). The V1 responses were the weakest, and none of the curve amplitudes was higher than their shuffled controls. Figure 3L shows the comparison of amplitudes of these response curves. The DE orientation responses of V4 were significantly larger than those for V2 (paired t-test, P = 0.00084), but V2 was not significantly different from V1 (paired t-test, P = 0.06). The mean ratio of the DE response amplitudes for V4:V2:V1 was 1:0.43:0.19.

If the patterns we obtained in V4 indeed reflect the property of DE orientation selectivity, then they should tolerate changes in noncritical parameters in the visual stimuli. We imaged DE maps for various parameters (different RD motion axes, different absolute disparity signs, different magnitudes of relative disparity steps, and different DE spatial frequencies), and we found that the strength of the patterns had some variations when the parameter values changed, but the spatial layout and the locations of domains were generally unaffected by the changes in these visual parameters (Fig. S7). Furthermore, DE orientation maps, similar to LE orientation maps, could be repeatedly imaged in different imaging sessions (days), and the orientation patterns were stable over time (Fig. S8). All of these data indicate that the DE map is indeed the intrinsic functional architecture of V4.

So far, we have shown that under anesthesia, V4 contained orientation maps for DE. We wondered whether these V4 maps only existed under anesthesia. We further performed the same imaging on an awake monkey performing a standard fixation task. Figure 4A,B shows the stimulus illustration and imaging time course. The visual stimuli were similar to those used in the anesthetized experiments, except that a dichoptic view was achieved by using a pair of LCD shutter glasses. Figure 4C shows a 0° versus 90° DE orientation map in which V4 exhibited a clear map for the DE orientation. The spatial pattern of this V4 map was similar to the pattern in the corresponding LE orientation map (Fig. 4D). The response profiles showed significant DE responses in V4 but not in V2 (Fig. 4E). The absence of orientation patterns in V1 and V2 in the LE orientation map (Fig. 4D) might be due to the lower map quality in the awake imaging. In addition, the V1/V2 regions in the imaging window were closer to the fovea (0°–1.5°) than the exposed V4 regions (0°–10°). The V1 region close to the fovea normally had a weaker orientation map (in both awake and anesthetized imaging), which was further reduced in awake imaging due to the presence of the fixation point (size: 0.3°).

Controls for DE maps

To exclude the possibility that these DE response patterns were due to monocular orientation cues, we repeated the imaging with monocular stimulation: in each condition, we only presented either the left-eye or the right-eye patch from a regular DE stimulus. Other stimulus parameters were the same as the regular DE stimuli, and thus, the number of stimulus conditions was doubled. We found that the V4 DE patterns were no longer elicited (Fig. 5B) and confirmed that there were no monocular orientation cues in the DE stimuli we used.

Our main DE stimuli contained binocularly matched-RD strips (zero disparity) separated by disparity strips. It is possible that this binocular matching information (not relative disparity) contributed to the DE response we observed. To eliminate this possibility, we tested stimuli containing binocularly matched and unmatched RD strips. The unmatched strips were binocularly uncorrelated RDs, separated by matched-RD strips (zero
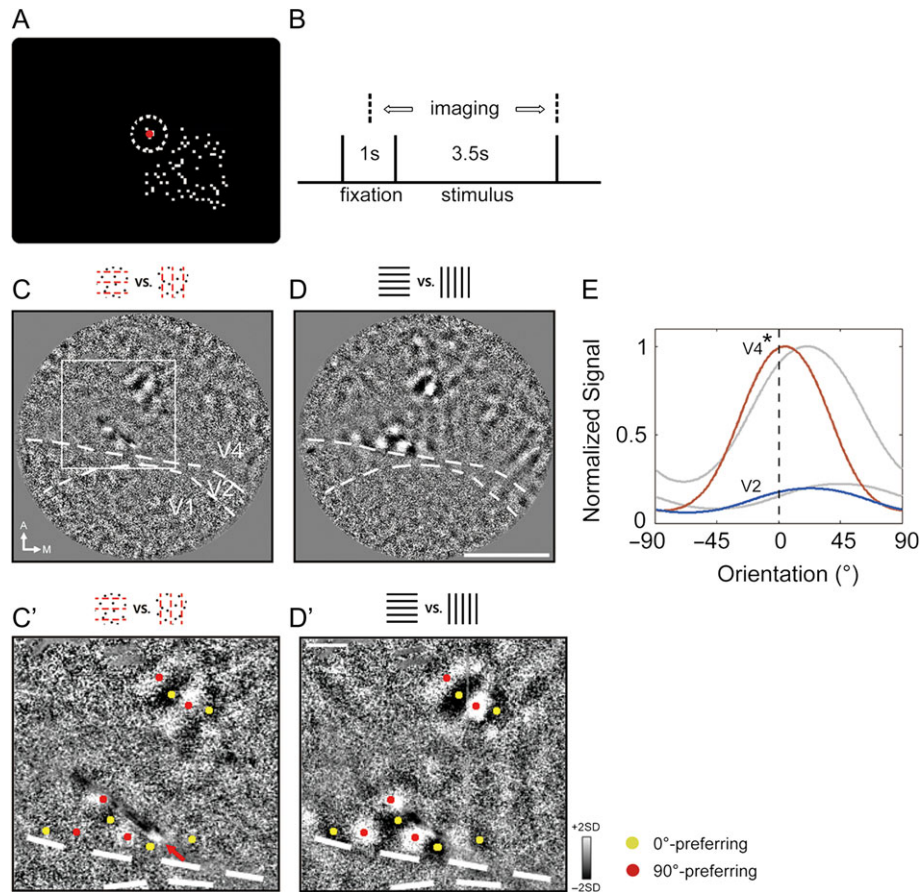
Figure 4. DE orientation maps imaged in an awake monkey. (A) Illustration of visual stimulus used in awake monkey imaging. The monkey viewed the stimulus through an LCD shutter goggle for a stereoscopic view. The red dot is the fixation spot. Dashed circle: fixation window (1.5° in diameter). (B) Timeline for stimulus presentation and imaging. The monkey's eyes were initially fixated on the fixation dot for 0.5 s, which triggered the imaging acquisition. After another 0.5 s of fixation, the RD stimulus appeared on the screen and lasted for 3.5 s. The total image acquisition time was 4 s. (C) A 0° versus 90° orientation map for the DE stimuli was imaged from the awake monkey (Case 5). Similar to the anesthetized cases, clear orientation patterns are observed in V4. (D) A 0° versus 90° orientation map for the LE stimuli was imaged on the same day as C. Similar orientation patterns are observed in V4. (C' and D') Magnified views of the V4 region framed in C. Yellow and red dots mark the gravity centers of the 0° and 90° orientation domains (LE orientation domain center identified from D' and transferred to C'). Two types of orientation maps in V4 showed generally similar activation patterns except that the responses in the lower V4 were weak (e.g., the bottom dots in C') and do not show clear domains corresponding with the LE domains. There was also noise from a surface blood vessel (red arrow in C'). Overall, these observations are consistent with those from the anesthetized monkey experiments. (E) Response profiles for the DE orientation patterns shown in C (colored) and another map not shown (gray). Only the V4 responses are significantly larger than the shuffled control. Scale bar in D: 5 mm, applies to C and D. Scale bar in D': 1 mm, applies to C' and D'.

disparity). Perceptually, strips still could be observed in these stimuli but were much weaker than the DE. Orientation maps obtained with such stimuli were weak (Fig. 5E) compared with normal DE maps obtained in the same imaging run (Fig. 5D). The response profiles and population results shown in Figure 5F also confirmed this observation. Although the quantitative analysis showed some weak orientation responses (2 cases, one significant and one nonsignificant), they were much weaker than the DE stimuli (consistent with perceptual impression). Thus, the alternative existence/nonexistence of binocular matching (or absolute disparity) may have weakly contributed to the DE orientation responses we observed, but such information alone was not enough. The disparity (or more specifically, relative disparity) was the main carrier of the edge information that elicited the orientation responses we observed.

In our imaging experiments, we also tested DE stimuli with vertical disparity. The stimuli were constructed in the same way as the DE stimuli, but the RD shifted vertically. We found that vertical disparity did not elicit orientation responses (Fig. 5H), while normal horizontal shift DE maps were obtained

in the same imaging run (Fig. 5G). A comparison of 2 response profiles is shown in Figure 5I. This is consistent with previous findings that horizontal and vertical disparities are not symmetrically represented in the visual cortex and that disparity neurons are specialized for processing horizontal disparity (Cumming 2002). This evidence also indicates that simple matching information is not sufficient and that horizontal disparity is indispensable in obtaining DE orientation responses.

Previous studies have shown that eye corresponding problems are progressively resolved along the ventral pathway (Janssen et al. 2003; Tanabe et al. 2004; Abdolrahmani et al. 2016; Fujita and Doi 2016; Verhoef et al. 2016; Chen et al. 2017). In V4, although responses to anti-correlated RD (aRD) are substantially reduced, most disparity neurons still show some disparity tuning to aRD stimuli (Tanabe et al. 2004). To test whether V4 still responds to aRD at the population level, we imaged cortical responses to DE stimuli constructed with aRD. The stimuli were similar to those used in regular DE imaging, except that each half-image was composed of both black and
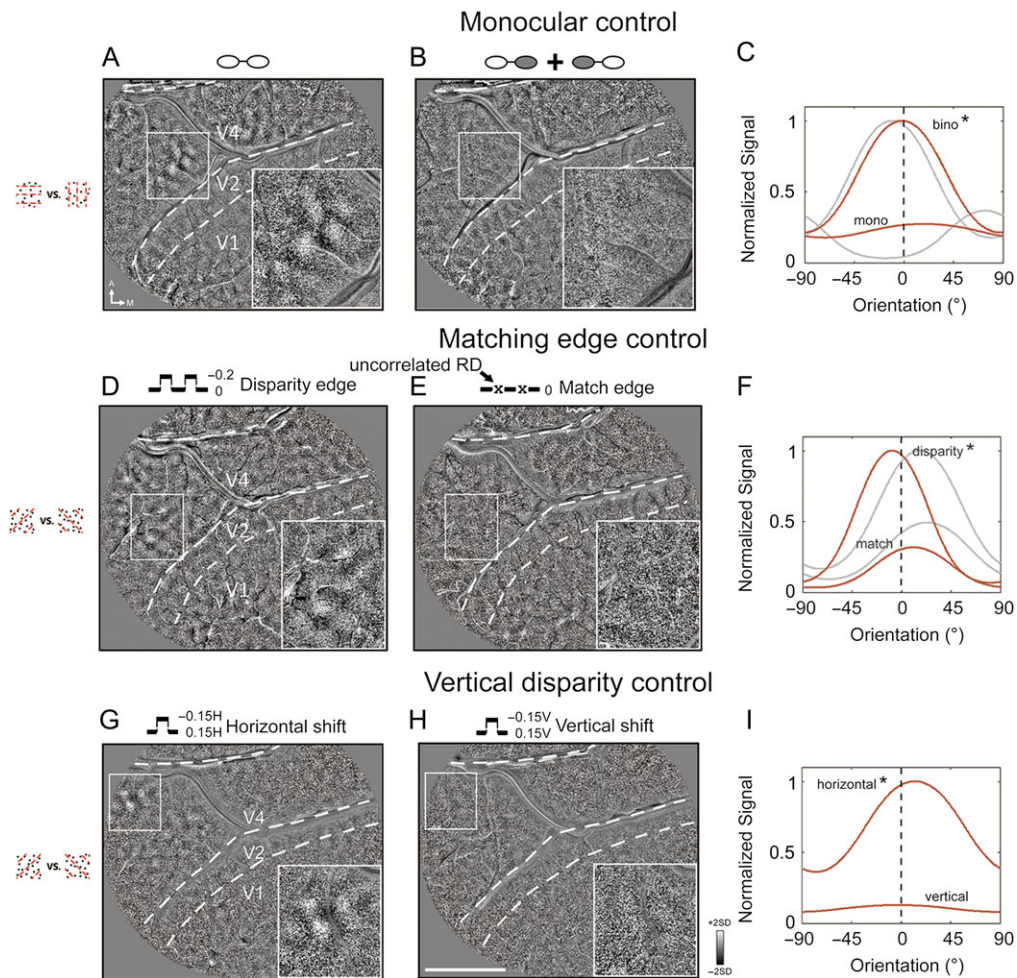
Figure 5. Negative controls for the DE orientation maps. (A) A regular DE orientation map from Case 1 shows orientation patterns in V4. The lower-right corners show a magnified view of a representative V4 region. (B) An orientation map obtained with monocular stimulation of the DE stimuli (the left-eye RD patch and right-eye RD patch were separately presented to 1 eye at a time in 2 stimulus conditions), which shows a flat map. These 2 maps were imaged in the same experiment run. (C) Response profiles for the V4 orientation responses shown in A and B (brown curves) and data from another case tested with the same binocular and monocular stimuli (gray curves, maps not shown). Curves from monocular controls are not significant. (D) A disparity-edge orientation map obtained with regular DE stimuli (0° and −0.2° disparity levels). (E) An orientation map obtained with binocular-matching edges. The matching-edge stimuli were similar to the DE stimuli, except that the RD strips normally containing disparity were replaced by nonmatching RDs (binocularly uncorrelated dots). These nonmatching RD strips were separated by 100% matching RD strips (zero disparity). Such a stimulus does not contain disparity edge information but contains match versus nonmatch edge information. The orientation maps obtained with such matching edges are mainly flat. (F) Response profiles for the V4 orientation responses shown in D and E (brown curves) and data from another case tested with the same disparity edge and match edge stimuli (gray curves, maps not shown). The orientation responses in the matching-edge maps are weak (2 cases, one curve significant, another nonsignificant). (G) A DE orientation map obtained with horizontal disparity stimuli. (H) Same imaging run; a DE orientation map obtained with DE stimuli that was constructed with vertical disparity (RDs shifted vertically). The map is mainly flat. (I) Response profiles for the 2 maps shown in G and H. The map obtained with vertical disparity is not significant. Scale bar in H: 5 mm, applies to A, B, D, E, G, and H.

white RD on a gray background (Fig. 6A,B). We tested both correlated and anti-correlated versions of DE stimuli in the same imaging run. Figure 6C–F shows the results obtained in one case and the population results. It can be seen that compared with a DE map obtained with correlated RD (Fig. 6C,C′,E), the map obtained with aRD was mainly flat (Fig. 6D,D′,F). Thus, although individual V4 neurons still have residual tuning to disparity in aRD stimuli (Tanabe et al. 2004), as a population, their responses to aRD DE stimuli were not observed.

Near-far disparity map in V4
Near-far disparity maps have been observed in V2 (Chen et al. 2008) and MT (DeAngelis and Newsome 1999). Previous single-cell recordings have also suggested that disparity neurons in V4 are clustered (Watanabe et al. 2002; Tanabe et al. 2005). We

were interested to see whether a near-far disparity map also existed in V4. With similar stimuli used in a previous publication (Chen et al. 2008, also see Fig. 7A), we imaged cortical responses to different levels of disparity in areas V1, V2 and V4 in 3 cases. However, in none of these cases did we observe a clear map for near-far disparity in area V4, despite the fact that disparity maps in V2 were presented in the same imaging windows (black arrows, Fig. 7B–D). Additionally, a map contrasting "near and far disparity" conditions and the "zero disparity" condition was also flat in V4 (data not shown).

Discussion

With intrinsic signal optical imaging, we showed that neurons preferring the same orientation of disparity-defined edges clustered in area V4 and formed an orientation map that co-
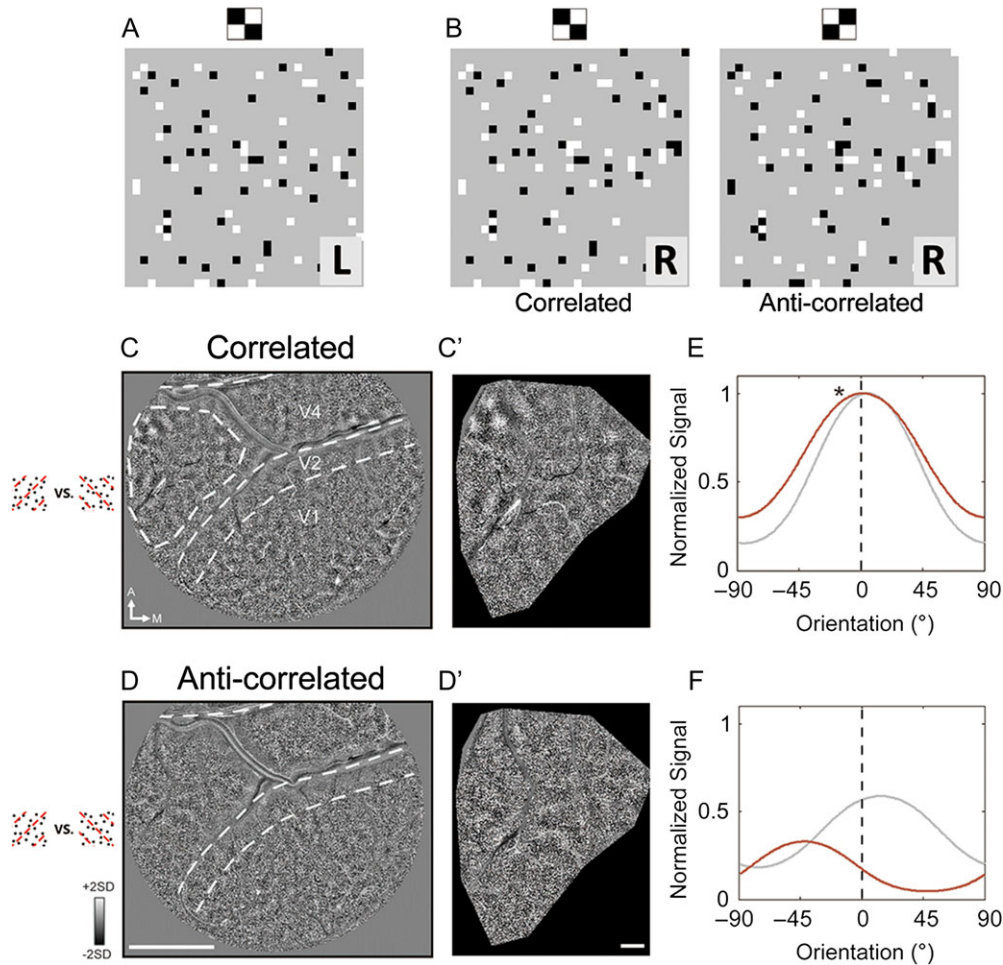
Figure 6. Absence of an orientation pattern in DE orientation maps obtained with anti-correlated DE stimuli. (A and B) Illustrations of DE stimuli constructed with correlated and anti-correlated RDs. A illustrates a left-eye stimulus patch, and the 2 patches in B are right-eye stimulus in 2 conditions in which RD patterns are either positively correlated (left panel: correlated) or negatively correlated (right panel: anti-correlated) with the left-eye stimulus in A. (C) A DE orientation map obtained with correlated DE stimuli from Case 1. C′ is a magnified view of a region in V4 (outlined in C). Similar to previous imaging, it shows orientation-preferring patterns. (D) A DE orientation map obtained with anti-correlated DE stimuli from the same experiment as C. The map is mainly flat. D′ is magnified views of the region in D outlined in C. (E and F) Response profiles for the corresponding V4 orientation maps on the left for correlated (E) and anti-correlated (F) DE maps (brown curves) as well as the results from another case (gray curves, maps not shown). Consistent with the map observation, correlated RD stimuli elicited an orientation response in V4 while anti-correlated stimuli did not. Scale bar in D: 5 mm, applies to C and D. Scale bar in D′: 1 mm, applies to C′ and D′.

localized with the orientation map for luminance-defined edges. These maps were not due to monocular cues and could be repeatedly imaged from the same cortical regions in both anesthetized and awake monkeys. Changes in noncritical parameters in the visual stimuli did not change these patterns, while using aRD no longer elicited them. In contrast, such maps were much weaker in V2 and totally absent in V1.

Coding of DE

Neurons sensitive to DE first emerge in area V2, although the presence of DE orientation selectivity in V1 was also reported (Gonzalez et al. 2007). They exhibit similar orientation-selectivity to both DE and LE, and thus, their orientation selectivity is cue invariant (von der Heydt et al. 2000; Qiu and von der Heydt 2005; Gonzalez et al. 2007). These V2 DE neurons may simply combine V1 inputs within their RF in a linear way (Bredfeldt and Cumming 2006; Bredfeldt et al. 2009). In the downstream area V4, neurons sensitive to DE have not been demonstrated so far, but fMRI evidence shows that activation by DE progressively increases along

the visual hierarchy (Tsao et al. 2003). The present study provides the first evidence showing that there are orientation-preferring responses in V4 for disparity-defined edges. An orientation map for DE is also the first direct evidence of a function structure for shape-from-disparity processing.

Our data reveal that DE responses are progressively strengthened along the V1–V2–V4 pathway (Fig. 3I–L). In area V1, neither the map observation nor the quantification analysis showed DE activation. In area V2, although a clear DE orientation map was not observed, some isolated domain activation could be identified, and quantification also showed significant DE orientation tuning (Figures 2 and 3). In area V4, a clear DE orientation map was observed and co-localized with the V4 LE orientation map. Such progressive differences suggest that V4 may contain more DE-responsive neurons than V2 or that DE selectivity in V4 neurons is more explicit.

The first emergence of clear DE orientation maps in area V4 suggests that V4 plays an important role in extracting edge information from disparity cues and may eventually contribute to shape-from-disparity perception. The co-localization of the DE
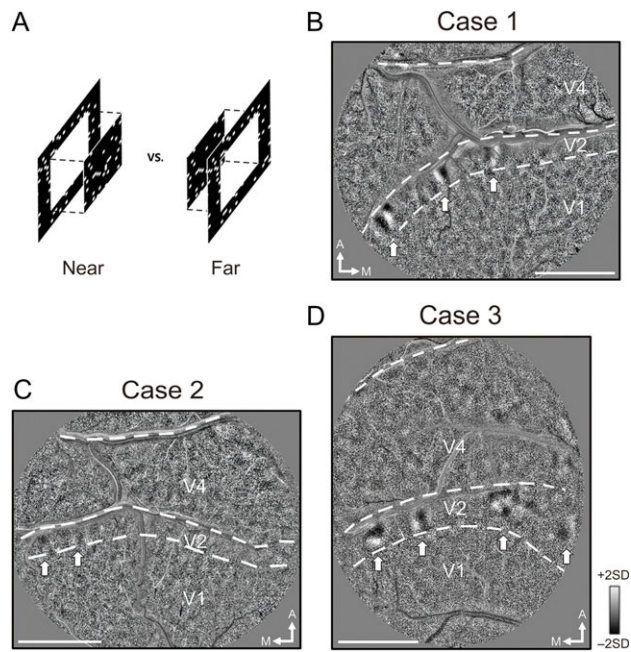
Figure 7. Absence of a near-far disparity map in V4. (*A*) An illustration of a pair of near and far stimuli used in pure disparity comparison (−0.2° vs. +0.2°). The RD patterns contained an 8° × 8° center (with disparity modulation) and a 10° × 10° surround part (fixed at zero disparity). (*B–D*) Near-far disparity maps obtained from Case 1 to Case 3. No obvious disparity patterns were observed in areas V1 and V4. Consistent with previous reports (Chen et al. 2008), clear disparity patterns were observed in area V2 in all 3 cases (white arrows). Disparity RDs are either drifting (*B*) or refreshed by new RD patterns at 10 Hz (*C* and *D*). Other parameters for random dots are the same as in the DE stimuli. Scale bar in *B*, *C*, *D*: 5 mm.

and LE orientation maps suggests that this shape-from-disparity can be combined with shape information derived from other cues (e.g., luminance, color, and motion cues). The orientation maps for some of these cues have already been observed in V4 (e.g., illusory contours in Pan et al. 2012). The present results expand these findings by indicating that V4 is an important stage in combining different types of cues for form/shape detection (e.g., luminance and disparity cues). The existence of a DE orientation map in V4 also facilitates future studies in quantitative measurements of cortical activation to shape-from-disparity. For example, one can measure the DE map strength and its relationship with animal behavioral performance in detecting DEs.

Coding of Disparity in V4

V4 plays an important role in processing binocular disparity information. Approximately 50–80% of V4 neurons are disparity sensitive (Hinkle and Connor 2001; Tanabe et al. 2005). These neurons show a bias towards crossed (near) disparity (Hinkle and Connor 2001; Tanabe et al. 2005), and most show a certain degree of coding of relative disparity, that is, their disparity tuning is modulated by the surround depth (Umeda et al. 2007). Although their relative disparity coding is not complete, it is improved over those observed in V2 (Thomas et al. 2002). Disparity information in V4 is likely used for detecting fine structures of objects (Tanabe et al. 2005) and underlies fine disparity discrimination (Shiozaki et al. 2012).

With surface disparity stimuli, we did not find a near-far disparity map in V4, although such maps were observed in V2 in

the same imaging window (Fig. 7). There are several possible reasons. First, the clustering may be weak or mainly located in deep layers. The primary evidence of clustering is the correlation of disparity tuning between single-unit and multi-unit recordings from the same electrode (Tanabe et al. 2005). Such correlation is the same for areas V1 and V4 (both correlation = 0.3, see Prince et al. 2002; Tanabe et al. 2005). Consistently, neither area shows a disparity map in our images. In comparison, the correlation is much higher in MT (correlation = 0.91), where disparity maps were observed (DeAngelis and Newsome 1999). One fact worth noting is that V4 neurons cover a smaller range of disparity than V1/MT neurons, which may yield lower correlation values. Additionally, the correlation of the disparity discrimination index, a measurement of strength of disparity tuning, is similar for V4 (0.64, Tanabe et al. 2005) and MT (0.66, Prince et al. 2002) and larger than that of V1 (0.37, Prince et al. 2002). Second, it is possible that disparity neurons in V4 were suppressed by the large disparity stimuli size (Desimone and Schein 1987; Umeda et al. 2007). Our imaging stimuli (10° × 10° patches) were larger than the stimuli used in single-cell recording studies (usually less than 5°). Although orientation and color maps were obtained with large stimuli, it is still possible that disparity neurons are more suppressed under such stimulus conditions. Additionally, large-stimulus suppression may also affect the orientation and color maps we obtained (Ghose and Ts'o 1997). Finally, there might be structures in area V4 that are organized by neurons selective to disparity that are associated with forms but not for plain disparity surfaces. Previous studies have shown that disparity tunings of most V4 disparity neurons are stimulus dependent. For example, one study found that most V4 cells (61%) had different disparity tuning profiles for bars and RDs (Hegde and Van Essen 2005). Thus, our disparity surface stimuli (Fig. 7A) might not effectively drive these neurons. We also do not exclude possibilities due to technical limitations of our imaging experiments. For example, neurons in the dorsal part of V4 are tuned to near disparities of less than 0.2°, which make these neurons more vulnerable to eye-alignment errors in anesthetized monkey experiments.

In contrast to a lack of basic near-far disparity functional architectures, neurons in V4 appear to cluster according to higher-order disparity information (disparity-defined edge orientation). This is consistent with the functional role of V4 in shape processing. For example, it has also been shown that V4 plays an important role in coding elements for 3D shapes, for example, 3D orientation (Hinkle and Connor 2002). Taken together, these findings suggest that disparity neurons in V4 are organized to detect intermediate elements for disparity-defined shapes, not according to their disparity response features per se.

Disparity Processing in the Dorsal and Ventral Pathways

Disparity neurons in V2 are mostly located in thick strips and form near/far disparity clusters (Hubel and Livingstone 1987; Chen et al. 2008; Ts'o et al. 2009), which mainly project to dorsal stream targets such as MT (DeYoe and Van Essen 1985; Shipp and Zeki 1985). Cooling studies also show that V2-MT projections mainly carry disparity information instead of motion (Ponce et al. 2008, 2011; Smolyanskaya et al. 2015). In the dorsal areas V3, V3A, and MT, most neurons exhibit disparity selectivity (DeAngelis et al. 1998; Adams and Zeki 2001; Anzai et al. 2011). In these areas, disparity neurons tend to cluster and form columnar organizations. Near-far disparity maps are found in area MT

(DeAngelis and Newsome 1999). Like in V1, neurons in these areas mainly code absolute disparities (DeAngelis et al. 1998; Anzai et al. 2011), although relative disparity coding has also been observed for specific types of stimuli (e.g., overlaid surfaces) in area MT (Krug and Parker 2011). These neurons mainly contribute to coarse disparity discrimination tasks (Uka and DeAngelis 2006; Chowdhury and DeAngelis 2008), for example, for guiding vergence control of the eyes (Neri 2005). However, MT and higher dorsal area (CIP, AIP) neurons are also sensitive to 3D surface orientation or concave/convex shapes (Xiao et al. 1997; Taira et al. 2000; Tsutsui et al. 2001; Nguyenkim and DeAngelis 2003; Srivastava et al. 2009; Verhoef et al. 2010) and depth separation (Duncan et al. 2000; Krug and Parker 2011; Krug et al. 2013; Sanada and DeAngelis 2014; Kim et al. 2015), which may contribute to surface representations.

Compared with neurons in the dorsal areas, disparity neurons in the ventral areas tend to emphasize relative disparity and fine disparity (Uka et al. 2005; Umeda et al. 2007; Shiozaki et al. 2012). These features are required for the 3D-shape representation of an object, a main function of the ventral pathway. Furthermore, responses to false matched (anti-correlated) disparity are gradually decreased along the ventral pathway and eliminated in area IT (Janssen et al. 2003; Tanabe et al. 2004; Abdolrahmani et al. 2016; Chen et al. 2017). Consistent with this general framework of dorsal/ventral functional segregation, our results show that in a typical ventral area V4, disparity information is effectively used for detection of object boundaries. Although V4 disparity neurons still show certain degrees of responses to aRD (Tanabe et al. 2004), V4 orientation neurons do not respond to false matched DEs (Fig. 6). This evidence suggests that the disparity-to-shape process in V4 selectively integrates meaningful information and rejects meaningless noise (false matching information). Such a process is likely carried out by relative disparity neurons, considering the fact that the disparity information in the DE stimuli is relative disparity in nature, as well as the fact that V4 disparity neurons are mainly sensitive to relative disparity (Umeda et al. 2007). Consistently, the negative control shows that the existence of matching information (or absolute disparity) alone did not elicit robust orientation responses (Fig. 5E).

Supplementary Material

Supplementary material is available at *Cerebral Cortex* online.

Funding

Notes

We thank RM Friedman for critical comments on the manuscript. Lab members J Lu, JW Pan, JJ Cai, C Xu, Z Yu, C Fang, XY Cai, and K Yan provided valuable technical assistance. *Conflict of Interest*: The authors declare no competing financial interests.

References

Abdolrahmani M, Doi T, Shiozaki HM, Fujita I. 2016. Pooled, but not single-neuron, responses in macaque V4 represent a solution to the stereo correspondence problem. J Neurophysiol. 115: 1917–1931.

Adams DL, Zeki S. 2001. Functional organization of macaque V3 for stereoscopic depth. J Neurophysiol. 86:2195–2203.

Anzai A, Chowdhury SA, DeAngelis GC. 2011. Coding of stereoscopic depth information in visual areas V3 and V3A. J Neurosci. 31:10270–10282.

Basole A, White LE, Fitzpatrick D. 2003. Mapping multiple features in the population response of visual cortex. Nature. 423:986–990.

Bosking WH, Zhang Y, Schofield B, Fitzpatrick D. 1997. Orientation selectivity and the arrangement of horizontal connections in tree shrew striate cortex. J Neurosci. 17:2112–2127.

Bredfeldt CE, Cumming BG. 2006. A simple account of cyclopean edge responses in macaque V2. J Neurosci. 26:7581–7596.

Bredfeldt CE, Read JCA, Cumming BG. 2009. A quantitative explanation of responses to disparity-defined edges in macaque V2. J Neurophysiol. 101:701–713.

Chen LM, Heider B, Williams GV, Healy FL, Ramsden BM, Roe AW. 2002. A chamber and artificial dura method for long-term optical imaging in the monkey. J Neurosci Methods. 113:41–49.

Chen M, Li P, Zhu S, Han C, Xu H, Fang Y, Hu J, Roe AW, Lu HD. 2016. An orientation map for motion boundaries in macaque V2. Cereb Cortex. 26:279–287.

Chen G, Lu HD, Roe AW. 2008. A map for horizontal disparity in monkey V2. Neuron. 58:442–450.

Chen G, Lu HD, Tanigawa H, Roe AW. 2017. Solving visual correspondence between the two eyes via domain-based population encoding in nonhuman primates. Proc Natl Acad Sci USA. 114:13024–13029.

Chowdhury SA, DeAngelis GC. 2008. Fine discrimination training alters the causal contribution of macaque area MT to depth perception. Neuron. 60:367–377.

Cumming BG. 2002. An unexpected specialization for horizontal disparity in primate primary visual cortex. Nature. 418:633–636.

DeAngelis GC, Cumming BG, Newsome WT. 1998. Cortical area MT and the perception of stereoscopic depth. Nature. 394:677–680.

DeAngelis GC, Newsome WT. 1999. Organization of disparity-selective neurons in macaque area MT. J Neurosci. 19: 1398–1415.

Desimone R, Schein SJ. 1987. Visual properties of neurons in area V4 of the macaque: sensitivity to stimulus form. J Neurophysiol. 57:835–868.

DeYoe EA, Van Essen DC. 1985. Segregation of efferent connections and receptive field properties in visual area V2 of the macaque. Nature. 317:58–61.

Duncan RO, Albright TD, Stoner GR. 2000. Occlusion and the interpretation of visual motion: perceptual and neuronal effects of context. J Neurosci. 20:5885–5897.

Essen DC, Zeki SM. 1978. The topographic organization of rhesus monkey prestriate cortex. J Physiol. 277:193–226.

Fujita I, Doi T. 2016. Weighted parallel contributions of binocular correlation and match signals to conscious perception of depth. Philos Trans R Soc Lond B Biol Sci. 371: 20150257. doi: 10.1098/rstb.2015.0257.

Ghose GM, Ts'o DY. 1997. Form processing modules in primate area V4. J Neurophysiol. 77:2191–2196.

Gonzalez F, Romero MC, Castro AF, Bermudez MA, Perez R. 2007. Sensitivity to direction and orientation of random dot stereobars in the monkey visual cortex. Eur J Neurosci. 25:2536–2546.

Hegde J, Van Essen DC. 2005. Stimulus dependence of disparity coding in primate visual area V4. J Neurophysiol. 93:620–626.

Hinkle DA, Connor CE. 2001. Disparity tuning in macaque area V4. Neuroreport. 12:365–369.

Hinkle DA, Connor CE. 2002. Three-dimensional orientation tuning in macaque area V4. Nat Neurosci. 5:665–670.

Hubel DH, Livingstone MS. 1987. Segregation of form, color, and stereopsis in primate area 18. J Neurosci. 7:3378–3415.

Janssen P, Vogels R, Liu Y, Orban GA. 2001. Macaque inferior temporal neurons are selective for three-dimensional boundaries and surfaces. J Neurosci. 21:9419–9429.

Janssen P, Vogels R, Liu Y, Orban GA. 2003. At least at the level of inferior temporal cortex, the stereo correspondence problem is solved. Neuron. 37:693–701.

Janssen P, Vogels R, Orban GA. 1999. Macaque inferior temporal neurons are selective for disparity-defined three-dimensional shapes. Proc Natl Acad Sci USA. 96:8217–8222.

Janssen P, Vogels R, Orban GA. 2000a. Selectivity for 3D shape that reveals distinct areas within macaque inferior temporal cortex. Science. 288:2054–2056.

Janssen P, Vogels R, Orban GA. 2000b. Three-dimensional shape coding in inferior temporal cortex. Neuron. 27:385–397.

Kamitani Y, Tong F. 2005. Decoding the visual and subjective contents of the human brain. Nat Neurosci. 8:679–685.

Kara P, Boyd JD. 2009. A micro-architecture for binocular disparity and ocular dominance in visual cortex. Nature. 458:627–631.

Kim HR, Angelaki DE, DeAngelis GC. 2015. A functional link between MT neurons and depth perception based on motion parallax. J Neurosci. 35:2766–2777.

Krug K, Cicmil N, Parker AJ, Cumming BG. 2013. A causal role for V5/MT neurons coding motion-disparity conjunctions in resolving perceptual ambiguity. Curr Biol. 23:1454–1459.

Krug K, Parker AJ. 2011. Neurons in dorsal visual area V5/MT signal relative disparity. J Neurosci. 31:17892–17904.

Li P, Zhu S, Chen M, Han C, Xu H, Hu J, Fang Y, Lu HD. 2013. A motion direction preference map in monkey V4. Neuron. 78: 376–388.

Lu HD, Chen G, Ts'o DY, Roe AW. 2009. A rapid topographic mapping and eye alignment method using optical imaging in Macaque visual cortex. Neuroimage. 44:636–646.

Neri P. 2005. A stereoscopic look at visual cortex. J Neurophysiol. 93:1823–1826.

Nguyenkim JD, DeAngelis GC. 2003. Disparity-based coding of three-dimensional surface orientation by macaque middle temporal neurons. J Neurosci. 23:7117–7128.

Pan Y, Chen M, Yin J, An X, Zhang X, Lu Y, Gong H, Li W, Wang W. 2012. Equivalent representation of real and illusory contours in macaque V4. J Neurosci. 32:6760–6770.

Parker AJ. 2007. Binocular depth perception and the cerebral cortex. Nat Rev Neurosci. 8:379–391.

Ponce CR, Hunter JN, Pack CC, Lomber SG, Born RT. 2011. Contributions of indirect pathways to visual response properties in macaque middle temporal area MT. J Neurosci. 31:3894–3903.

Ponce CR, Lomber SG, Born RT. 2008. Integrating motion and depth via parallel pathways. Nat Neurosci. 11:216–223.

Prince SJ, Pointon AD, Cumming BG, Parker AJ. 2002. Quantitative analysis of the responses of V1 neurons to horizontal disparity in dynamic random-dot stereograms. J Neurophysiol. 87:191–208.

Qiu FTT, von der Heydt R. 2005. Figure and ground in the visual cortex: V2 combines stereoscopic cues with Gestalt rules. Neuron. 47:155–166.

Ramsden BM, Hung CP, Roe AW. 2001. Real and illusory contour processing in area V1 of the primate: a cortical balancing act. Cereb Cortex. 11:648–665.

Sanada TM, DeAngelis GC. 2014. Neural representation of motion-in-depth in area MT. J Neurosci. 34:15508–15521.

Shiozaki HM, Tanabe S, Doi T, Fujita I. 2012. Neural activity in cortical area V4 underlies fine disparity discrimination. J Neurosci. 32:3830–3841.

Shipp S, Zeki S. 1985. Segregation of pathways leading from area V2 to areas V4 and V5 of macaque monkey visual cortex. Nature. 315:322–325.

Smolyanskaya A, Haefner RM, Lomber SG, Born RT. 2015. A modality-specific feedforward component of choice-related activity in MT. Neuron. 87:208–219.

Srivastava S, Orban GA, De Maziere PA, Janssen P. 2009. A distinct representation of three-dimensional shape in macaque anterior intraparietal area: fast, metric, and coarse. J Neurosci. 29: 10613–10626.

Taira M, Tsutsui KI, Jiang M, Yara K, Sakata H. 2000. Parietal neurons represent surface orientation from the gradient of binocular disparity. J Neurophysiol. 83:3140–3146.

Tanabe S, Doi T, Umeda K, Fujita I. 2005. Disparity-tuning characteristics of neuronal responses to dynamic random-dot stereograms in macaque visual area V4. J Neurophysiol. 94: 2683–2699.

Tanabe S, Umeda K, Fujita I. 2004. Rejection of false matches for binocular correspondence in macaque visual cortical area V4. J Neurosci. 24:8170–8180.

Tanaka H, Uka T, Yoshiyama K, Kato M, Fujita I. 2001. Processing of shape defined by disparity in monkey inferior temporal cortex. J Neurophysiol. 85:735–744.

Tanigawa H, Lu HD, Roe AW. 2010. Functional organization for color and orientation in macaque V4. Nat Neurosci. 13: 1542–1548.

Thomas OM, Cumming BG, Parker AJ. 2002. A specialization for relative disparity in V2. Nat Neurosci. 5:472–478.

Tsao DY, Vandluffel W, Sasaki Y, Fize D, Knutsen TA, Mandeville JB, Wald LL, Dale AM, Rosen BR, Van Essen DC, et al. 2003. Stereopsis activates V3A and caudal intraparietal areas in macaques and humans. Neuron. 39:555–568.

Tsutsui K, Jiang M, Yara K, Sakata H, Taira M. 2001. Integration of perspective and disparity cues in surface-orientation-selective neurons of area CIP. J Neurophysiol. 86:2856–2867.

Ts'o DY, Frostig RD, Lieke EE, Grinvald A. 1990. Functional organization of primate visual cortex revealed by high resolution optical imaging. Science. 249:417–420.

Ts'o DY, Zarella M, Burkitt G. 2009. Whither the hypercolumn? J Physiol. 587:2791–2805.

Uka T, DeAngelis GC. 2006. Linking neural representation to function in stereoscopic depth perception: roles of the middle temporal area in coarse versus fine disparity discrimination. J Neurosci. 26:6791–6802.

Uka T, Tanabe S, Watanabe M, Fujita I. 2005. Neural correlates of fine depth discrimination in monkey inferior temporal cortex. J Neurosci. 25:10796–10802.

Uka T, Tanaka H, Yoshiyama K, Kato M, Fujita I. 2000. Disparity selectivity of neurons in monkey inferior temporal cortex. J Neurophysiol. 84:120–132.

Umeda K, Tanabe S, Fujita I. 2007. Representation of stereoscopic depth based on relative disparity in macaque area V4. J Neurophysiol. 98:241–252.

Verhoef BE, Vogels R, Janssen P. 2010. Contribution of inferior temporal and posterior parietal activity to three-dimensional shape perception. Curr Biol. 20:909–913.

Verhoef BE, Vogels R, Janssen P. 2016. Binocular depth processing in the ventral visual pathway. Philos Trans R Soc Lond B Biol Sci. 371: 20150259. doi:10.1098/rstb.2015.0259.

von der Heydt R, Zhou H, Friedman HS. 2000. Representation of stereoscopic edges in monkey visual cortex. Vision Res. 40: 1955–1967.

Watanabe M, Tanaka H, Uka T, Fujita I. 2002. Disparity-selective neurons in area V4 of macaque monkeys. J Neurophysiol. 87:1960–1973.

Xiao DK, Marcar VL, Raiguel SE, Orban GA. 1997. Selectivity of macaque MT/V5 neurons for surface orientation in depth specified by motion. Eur J Neurosci. 9:956–964.

Xiao Y, Rao R, Cecchi G, Kaplan E. 2008. Improved mapping of information distribution across the cortical surface with the support vector machine. Neural Netw. 21:341–348.

Xu H, Han C, Chen M, Li P, Zhu S, Fang Y, Hu J, Ma H, Lu HD. 2016. Rivalry-like neural activity in primary visual cortex in anesthetized monkeys. J Neurosci. 36:3231–3242.

Yoshiyama K, Uka T, Tanaka H, Fujita I. 2004. Architecture of binocular disparity processing in monkey inferior temporal cortex. Neurosci Res. 48:155–167.